中图法分类号:TP391　　**文献标识码**: A　　**文章编号**: 1006-8961(XXXX)XX-0001-14

论文引用格式:Zhou Hao, Shi Yuhang, Zhang Qian, Tao Tao, Guan Xin. Remote sensing image dehazing network via dynamic multi-expert gating[J/OL]. Journal of Image and Graphics, XXXX:1-14. DOI: 10.11834/jig.250646. (周昊, 施宇航, 张骞, 陶陶, 关鑫. 融合动态多专家门控的遥感图像去雾网络[J/OL]. 中国图象图形学报,XXXX:1-14. DOI: 10.11834/jig.250646.)[DOI:10.11834/jig.250646]

融合动态多专家门控的遥感图像去雾网络

周昊[1,2],施宇航[1],张骞[1],陶陶[1*],关鑫[3]

1. 安徽工业大学计算机科学与技术学院,马鞍山　243000; 2. 多模态认知计算安徽省重点实验室(安徽大学),合肥　230601; 3. 西南大学计算机与信息科学学院,重庆　400715

摘　要: 目的　针对复杂大气条件下遥感图像中的雾分布高度非均匀、颜色失真严重以及结构细节易丢失等问题,研究一种具备动态特征建模能力的遥感图像去雾方法,以提升模型在真实场景中的稳定性与泛化性。**方法**　在U-Net框架基础上,提出一种基于动态多专家门控机制的遥感图像去雾网络(dynamic multi-expert gating dehazing network,DMEGD-Net)。通过构建由颜色专家与边缘专家组成的多专家分支,并引入动态门控网络实现特征的自适应加权融合,增强模型对不同雾分布与地物特征的建模能力。同时,利用通道-像素注意力模块以强化关键通道与空间位置的响应,在解码阶段使用双源融合模块以协同整合高层语义信息与低层结构细节。此外,构建结合内容一致性与边缘结构约束的复合损失函数,引导网络在去雾中兼顾整体视觉质量与局部结构恢复。**结果**　在SateHaze1k、HRSD和RRSHID的多个遥感图像去雾数据集上的实验结果表明,所提方法在峰值信噪比(peak signal-to-noise ratio,PSNR)、结构相似性指数(structural similarity index measure, SSIM)和雾密度感知评价指标FADE(fog aware density evaluator, FADE)的客观评价指标上均取得优于现有主流方法的去雾质量表现。在SateHaze1k浓雾场景中,本文方法的PSNR达22.32dB、SSIM达0.8441,相较AU-Net分别提升12.4%和2.6%,FADE指标低至0.22,有效抑制残留雾感,提升结构一致性和颜色还原效果。消融实验进一步验证了动态多专家门控机制、注意力模块及复合损失函数在性能提升中的有效性。**结论**　本文所提出DMEGD-Net能够显著增强遥感图像去雾模型对复杂场景的自适应能力,为高质量遥感图像去雾提供了一种有效解决方案。代码与模型已公开:https://github.com/YuH1127/DMEGD-Net或者https://doi.org/10.57760/sciencedb.j00240.00054。

关键词: 图像去雾;遥感图像;动态门控机制;多专家网络;卷积神经网络

Remote sensing image dehazing network via dynamic multi-expert gating

Zhou Hao[1,2], Shi Yuhang[1], Zhang Qian[1], Tao Tao[1*], Guan Xin[3]

1. School of Computer Science and Technology, Anhui University of Technology, Ma'anshan 243032, China; 2. Anhui Provincial Key Laboratory of Multimodal Cognitive Computation, Anhui University, Hefei 230601, China; 3. College of Computer and Information Science, Southwest University, Chongqing 400715, China

Abstract: Objective Remote sensing images acquired under complex atmospheric environments are frequently affected by haze, thin clouds, and aerosol scattering, leading to severe degradation in visual quality and information fidelity. Such degradations manifest as reduced contrast, color distortion, blurred boundaries, and loss of fine structural details, which sig-

收稿日期:2025-12-24;**修回日期**:2026-03-13

*通信作者:陶陶,男,教授,博士研究生,主要研究方向为嵌入式系统与数据隐私保护。 E-mail:taotao@ahut.edu.cn

基金项目:国家自然科学基金项目(62401012);多模态认知计算安徽省重点实验室(安徽大学)开放基金(MMC202509)

Supported by: National Natural Science Foundation of China(62401012); The Open Project of Anhui Provincial Key Laboratory of Multimodal Cognitive Computation, Anhui University, No. MMC202509

nificantly compromise the reliability of downstream remote sensing applications, including land-cover classification, urban monitoring, object detection, and disaster assessment. Although substantial progress has been made in image dehazing over the past decade, most existing approaches are primarily developed for natural images and exhibit limited adaptability when applied to remote sensing data. Unlike natural images, remote sensing images are characterized by large spatial coverage, diverse land-cover distributions, complex textures, and highly non-uniform haze patterns caused by varying terrain and atmospheric conditions. In particular, many deep learning-based dehazing models rely on static network architectures and fixed feature fusion strategies, which lack the flexibility to dynamically respond to spatially varying haze densities and heterogeneous scene structures. Consequently, these methods often suffer from over-smoothing, incomplete haze removal, or color inconsistencies in real-world remote sensing scenarios. To address these challenges, the objective of this study is to develop an adaptive remote sensing image dehazing framework with enhanced feature modeling capability, capable of dynamically adjusting its representation according to local atmospheric conditions and scene characteristics, thereby improving robustness, stability, and generalization performance across diverse haze scenarios. **Method** To achieve this objective, we propose a novel dynamic multi-expert gating dehazing network (DMEGD-Net) based on a U-Net encoder-decoder architecture. Unlike existing based on U-Net architecture dehazing models that rely on a single static feature extraction, the proposed network introduces a dynamic multi-expert modeling paradigm that explicitly decomposes feature learning into complementary sub-tasks. Specifically, a dynamic multi-expert gating (MEG) is designed, consisting of a color expert and an edge expert, each specializing in different aspects of haze degradation. The color expert employs a 1×1 convolutional layer to effectively capture inter-channel correlations and restore chromatic consistency distorted by atmospheric scattering, while the edge expert utilizes a 3×3 convolutional layer to emphasize spatial structures and high-frequency details critical for preserving object boundaries and textures. A key innovation of DMEGD-Net lies in its learned gating mechanism, which dynamically predicts adaptive fusion weights for the two experts based on the input feature representations. This gating strategy enables the network to selectively emphasize color-oriented or structure-oriented features at different spatial locations, allowing for flexible adaptation to non-uniform haze distributions. Compared with fixed fusion strategies, the proposed dynamic gating mechanism provides enhanced modeling capacity for complex remote sensing scenes. Furthermore, a channel-pixel attention (CPA) is introduced to jointly model channel-wise importance and pixel-level spatial saliency. By suppressing haze-dominated responses and enhancing informative regions, the CPA enables fine-grained feature refinement and improves the discrimination of haze-free structures. To facilitate accurate image reconstruction, a dual-source fusion block (DFB) is incorporated into the decoder to explicitly integrate high-level semantic features from deep layers with low-level structural details from shallow layers, effectively alleviating edge blurring and texture loss commonly observed in dehazing tasks. In addition, a content-edge composite loss function is formulated to jointly enforce global appearance consistency and local structural fidelity. This loss function combines a content reconstruction term with an edge-preserving constraint, providing explicit supervision for recovering sharp edges while maintaining overall visual realism. **Result** Extensive experiments are conducted on three representative remote sensing image dehazing datasets, namely SateHaze1k, HRSD, and RRSHID, which include both synthetic and real-world haze scenarios with varying haze densities and scene complexities. The proposed DMEGD-Net is evaluated using both full-reference metrics, including peak signal-to-noise ratio (PSNR) and structural similarity index measure (SSIM), as well as the no-reference fog aware density evaluator (FADE), ensuring a comprehensive and objective assessment of dehazing performance. Quantitative results demonstrate that DMEGD-Net consistently outperforms existing state-of-the-art dehazing methods across all datasets and haze levels. In particular, on the SateHaze1k dataset, the proposed method achieves a significant improvement in average PSNR compared with AU-Net, which is also based on a U-Net framework, with an increase of approximately 13.8%. Notably, the performance gains become more pronounced under moderate and heavy haze conditions, where spatially non-uniform haze poses substantial challenges to conventional methods. The proposed model also achieves superior SSIM, indicating improved structural consistency, and lower FADE values, reflecting more effective haze removal without introducing excessive artifacts. Qualitative comparisons further confirm that the DMEGD-Net produces visually more natural dehazed images, characterized by more accurate color restoration, clearer structural details, and reduced residual haze. In real remote sensing scenarios, the proposed method demonstrates strong robustness in handling heterogeneous land-cover types

and complex atmospheric effects, outperforming competing approaches that often suffer from color shifts, over-smoothing, or incomplete haze removal. Ablation studies systematically validate the effectiveness of each proposed component, showing that the dynamic multi-expert gating mechanism, the attention module, the dual-source fusion strategy, and the composite loss function all contribute substantially to the overall performance improvements. **Conclusion** This study presents an adaptive and effective solution for remote sensing image dehazing by introducing a dynamic multi-expert gating paradigm into deep convolutional networks. By explicitly modeling and dynamically balancing color and structural information, the proposed DMEGD-Net overcomes the limitations of static architectures when dealing with complex and non-uniform haze conditions. The integration of attention-guided feature enhancement and multi-level feature fusion further strengthens the network's ability to recover fine details and preserve structural consistency, leading to superior performance in both objective evaluation metrics and subjective visual quality. Although the proposed method achieves significant performance improvements, the dynamic multi-expert design introduces additional computational complexity, which may affect efficiency in large-scale or resource-constrained applications. Future work will focus on lightweight network design, incorporating physical atmospheric constraints to improve interpretability, and extending the proposed dynamic expert modeling strategy to other remote sensing image restoration tasks such as denoising, super-resolution, and cloud removal. Overall, this work highlights the potential of dynamic multi-expert learning as a promising direction for robust, generalizable, and high-quality remote sensing image enhancement. Code is available: https://github. com/YuH1127/DMEGD-Netorhttps://doi. org/10. 57760/sciencedb. j00240. 00054.

Key words: image dehazing; remote sensing; dynamic gating; multi-expert network; convolutional neural network

0 引　言

遥感图像作为地表信息获取的重要数据源，在土地利用与覆盖变化监测、城市精细化管理、目标检测以及灾害应急评估等领域发挥着关键作用。然而，在雾霾、薄云等复杂大气条件影响下，大气中的气溶胶粒子对电磁波产生散射与吸收作用，导致遥感图像对比度下降、结构细节减弱，并伴随明显的颜色偏移，从而严重影响后续高层视觉任务的准确性与可靠性(Koschmieder，1924；Gao等，2020)。因此，在雾分布高度非均匀的条件下实现高质量遥感图像去雾，仍是图像处理与遥感领域亟待解决的重要问题(Tang等，2022)。

围绕图像去雾问题，早期研究主要集中于图像增强与物理建模的方法。基于图像增强的方法通过调整图像亮度、对比度或颜色分布以改善视觉效果，例如直方图均衡化(Zuiderveld，1994)和多尺度Retinex模型(Jobson等，1997)。该类方法实现简单、计算效率高，但由于缺乏对雾形成机理的建模，在复杂场景下容易产生噪声放大和颜色失真等问题，难以满足遥感图像在实际应用中对结构真实性和辐射一致性的要求(Fu等，2016)。

为更准确地描述真实成像过程，研究者提出了基于物理先验的图像去雾方法，其核心是基于大气散射模型(atmosphere scattering model，ASM)(Koschmieder，1924)对图像退化过程进行建模，并通过估计透射率和大气光以实现图像恢复。典型方法包括暗通道先验(dark channel prior，DCP)(He等，2009)和颜色衰减先验(color attenuation prior，CAP)(Zhu等，2015)，这些方法在自然图像中取得了良好效果，并逐步应用与遥感图像处理(胡伟等，2010)。随后，基于非局部先验的去雾方法通过颜色聚类建模增强了对复杂场景的适应能力(Berman和Avidan，2016)，而基于异质大气光先验方法进一步考虑了光照的空间不均匀性(He等，2023)。然而，由于遥感图像通常具有视场范围大、地物类型复杂以及雾分布高度非均匀等特点，依赖统计假设的物理先验方法在细节恢复和色彩重建方面仍存在局限，容易产生结构伪影或辐射失真(Gao等，2020)。

随着深度学习技术的发展，基于卷积神经网络(convolutional neural network，CNN)的端到端去雾方法逐渐成为研究主流。例如，DehazeNet(Cai等，2016)通过学习从有雾图像到透射率的非线性映射实现单幅图像去雾；多合一去雾网络(all-in-one dehazing network，AOD-Net)(Li等，2017)将SAM参数统一为一体化映射函数，从而简化推理流程并提升模型鲁棒性。随后，多尺度特征提取和注意力机

制被广泛引入，以增强模型对复杂雾分布的表达能力，例如GridDehaze-Net（Liu等，2021）通过多尺度网格结构提升不同尺度雾信息的建模能力，特征融合注意力网络（feature fusion attention network，FFA-Net）（Qin等，2020）利用通道与像素级注意力机制增强了纹理细节恢复能力。

针对遥感图像高分辨率与复杂场景结构特点，研究者进一步提出了多种改进模型。例如，物理感知去雾网络（physic-aware dehazing network，PhD-Net）（Lihe等，2024）通过金字塔蒸馏融合多尺度特征，在性能与效率之间取得平衡；非对称式U-Net（asymmetric U-Net，AU-Net）（Du等，2024）在U-Net框架中引入注意力引导机制以增强结构重建能力；混合结构去雾网络（mixed structure dehazing network，MixDehazeNet）（Lu等，2024）通过混合结构模块加强多源特征交互。此外，结合物理约束与深度学习的混合方法也逐渐受到关注，在一定程度上提升了模型的可解释性和泛化能力（王炜嘉等，2025）。尽管这些方法在客观指标和视觉质量方面取得了显著进展，但在真实遥感场景中仍面临挑战：雾分布的强非均匀性使单一尺度或静态结构难以兼顾不同区域的去雾需求，同时高频纹理与复杂边缘在去雾过程中仍易被过度平滑，影响结构完整性。此外，多数模型采用静态结构，对不同雾强度和地物类型的自适应能力仍然有限（Zhu等，2025）。

为提升模型对复杂场景的适应能力，动态建模逐渐成为重要研究方向。其中，混合专家模型（mixture-of-experts，MOE）通过构建多个功能互补的专家分支，并利用门控机制根据输入特征进行动态选择，在自然语言处理和计算机视觉任务中展现出良好的泛化能力（Shazeer等，2017；Riquelme等，2021）。在图像去雾领域，多分支结构已被用于针对不同雾浓度或区域特性进行建模，例如基于雾浓度分类的多分支去雾网络在一定程度上提升了模型鲁棒性（张琪东等，2024）。然而，现有方法多依赖静态分支融合或先验规则驱动的分支选择策略，尚未充分挖掘动态多专家协同机制在遥感图像去雾中的潜力。

基于上述分析，本文在U-Net框架基础上引入动态多专家门控机制，构建一种面向遥感图像的动态多专家去雾网络。该方法通过多分支专家模块实现特征的自适应选择与融合，并结合注意力机制强化关键区域信息，同时利用高低层特征协同重建图像结构，从而在复杂雾条件下有效提升遥感图像的去雾质量与模型泛化能力。

1 本文方法

1.1 DMEDG-Net整体架构

如图1所示，DMEGD-Net整体架构基于U-Net，通过设计动态多专家门控模块（dynamic multi-expert gating，MEG）、通道-像素注意力模块（channel-pixel attention module，CPA）和双源融合模块（dual-source fusion block，DFB），以实现关键特征增强、冗余信息抑制以及结构与语义信息的深度融合，从而显著提升模型对遥感图像的去雾能力。在编码器阶段，有雾图像通过多次可变形卷积（linear deformable convolution，LD-Conv）（Zhang等，2024）及下采样操作后进入MEG，并由多个专家分支捕捉不同语义层次的上下文信息，通过门控机制实现加权融合。随后，CPA进一步提升模型对关键通道与空间细节的感知能力。在解码阶段，模型利用DFB整合跳跃连接传递的低层结构信息与上采样后的高层语义信息，从而有效恢复图像纹理和结构细节，最终生成结构清晰、色彩真实的去雾图像。

1.2 动态多专家门控模块

受MOE中“每个专家专注处理输入空间的特定区域”的启发，本文设计出MEG。假设MEG的输入特征为y，其被并行地传入门控网络、颜色专家分支E_1和边缘专家分支E_2。在门控网络中的全连接（Full Connect，FC）之前采用“3×3 Conv + BatchNorm + ReLU”的结构，以保留更多的空间上下文信息，并使得FC的输入更稳定（Jacobs等，1991；Hu等，2018）。专家分支均为“Conv + BatchNorm + ReLU”的结构，在Lin等人的工作中提出1×1卷积擅长跨通道混合与通道维变换，可以学习颜色通道之间的组合，所以E_1使用1×1卷积对每个空间位置的通道向量做线性投影捕获颜色信息（Lin等，2014）。浅层卷积核在训练后通常表现出有方向性的滤波器或者不同频率的纹理响应，所以E_2使用3×3卷积捕获边缘和局部结构（Matthew等，2013）。最后，MEG通过动态门控网络对各专家输出特征进行加权融合处理，从而实现自适应特征整合与信息调节，增强模型的表达能力与泛化能力，其过程可表示为

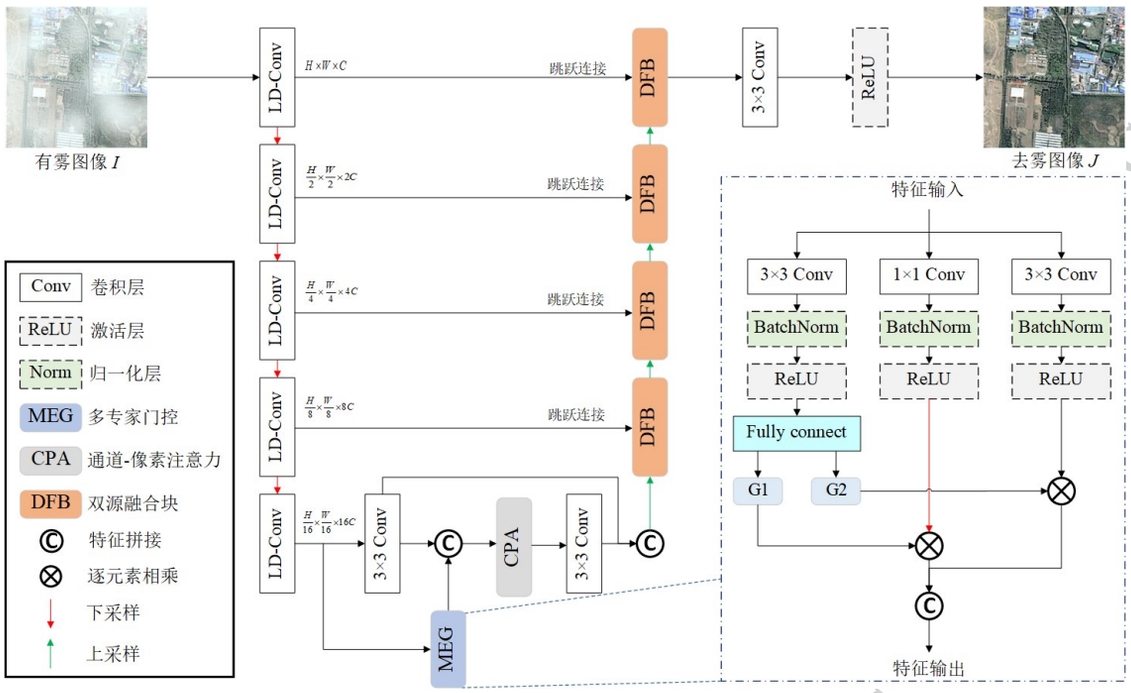

图 1　DMEGD-Net 模型整体结构图

Fig. 1　Overall architecture of the DMEGD-Net

$$\boldsymbol{y}_M = Concat(G_1 \otimes \boldsymbol{E}_1(\boldsymbol{y}), G_2 \otimes \boldsymbol{E}_2(\boldsymbol{y})) \quad (1)$$

式中，⊗代表逐元素相乘，G_1 和 G_2 并非人工经验设定的固定值，而是门控网络基于输入特征 $\boldsymbol{y}$ 自适应学习生成的权重，其数值大小由输入图像的雾分布特性与地物结构特征决定，以此实现对颜色专家和边缘专家输出特征的动态加权分配。$\boldsymbol{E1}(\boldsymbol{y})$ 和 $\boldsymbol{E2}(\boldsymbol{y})$ 分别为颜色专家和边缘专家的输出，$\mathbf{yM}$ 是该模块的最终输出特征。

1.3　通道-像素注意力模块

针对遥感图像中纹理复杂、结构多样的特点，本文设计 CPA 用于联合建模通道重要性与像素位置的重要性。该模块能够有效抑制雾主导的冗余响应，突出关键通道与像素区域，从而提升细节保留能力和结构一致性。模块结构如图 2 所示，通道注意力借助全局平均池化（global average pooling，GAP）和 1×1 卷积计算不同通道的响应强度，引导模型突出关键语义特征。像素注意力则通过卷积与激活操作对空间维度进行建模，聚焦图像局部区域细节，从而提升纹理保留能力。

1.4　双源融合模块

遥感图像在重建过程中，高层语义信息和低层结构信息同样重要，特别是对于地物边界、道路轮廓等区域，低层的结构细节对图像的恢复具有关键作用。为此，DFB 被设计并引入解码阶段对高层语义特征与低层细节特征进行协同建模。通过多尺度并行卷积与特征聚合，有效提升边缘与纹理的恢复质量，增强去雾图像结构真实性。模块结构如图 3 所示，DFB 接收两组特征输入：一是上采样得到特征

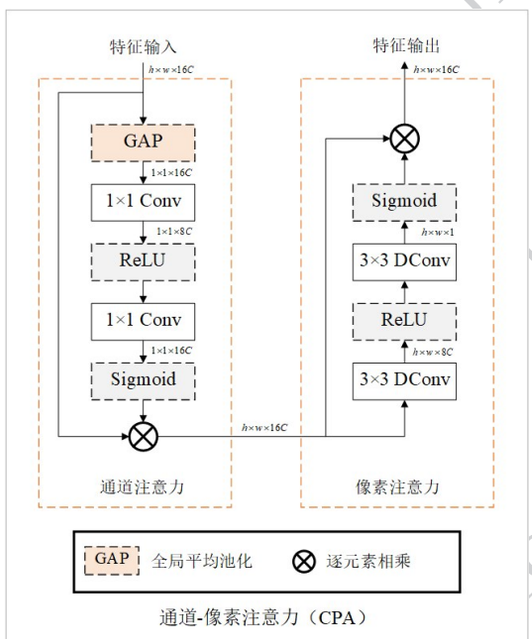

图 2　通道-像素注意力模块（CPA）的结构图

Fig. 2　Detailed architecture of the Channel-Pixel Attention module (CPA)

fup，二是跳跃连接的特征f_{skip}。将两组特征拼接后，首先通过1×1卷积$Conv_1$进行通道压缩与非线性激活，随后进入两个不同大小卷积（3×3卷积$Conv_3$和5×5卷积$Conv_5$）的并行分支以建模不同尺度的上下文信息，最后以逐元素相加的方式整合不同尺度的特征信息。其过程表示为

$$f = ReLU(Conv_1(Concat(\mathbf{fup}, \mathbf{fskip}))) \tag{2}$$

$$f_1 = ReLU(BN(Conv_3(f))) \tag{3}$$

$$f_2 = ReLU(BN(Conv_5(f))) \tag{4}$$

$$f_D = f_1 + f_2 \tag{5}$$

式中，f为通道压缩后的特征，f_1和f_2是f进入并行分支后得到不同尺度特征，f_D为DFB的最终输出。

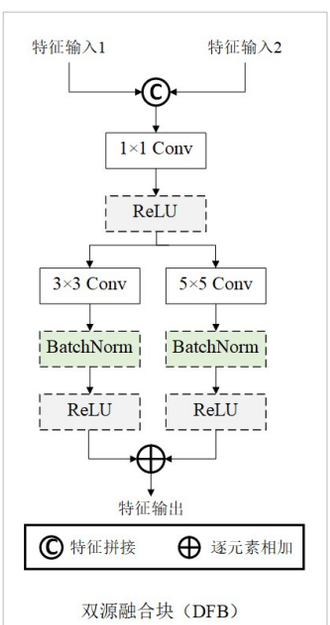

图3　双源融合模块（DFB）的结构图

Fig. 3　Detailed architecture of the Dual-source Fusion Block (DFB)

1.5　损失函数

为同时保证整体视觉质量与局部结构清晰度，本文构建结合内容一致性与边缘结构约束的复合损失函数Lce。内容损失Lc用于约束去雾图像与参考图像之间的整体差异，边缘损失Le则引导模型关注结构细节，有效提升去雾结果的感知质量。总损失函数定义为

$$L_ce = \lambda_1 \times L_c + \lambda_2 \times L_e \tag{6}$$

式中，λ_1和λ_2分别为两个子损失的权重系数，Lc采用均方误差（mean squared error，MSE）定义去雾图像$\boldsymbol{J}_{ed}$与清晰图像$\boldsymbol{J}$之间的内容差异，表示为

$$Lc = \left\| \boldsymbol{J}_{ed} - \boldsymbol{J} \right\|_2^2 \tag{7}$$

为强化边缘细节的学习，引入L_e，其定义为

$$Le = \left\| \theta(\boldsymbol{J}_{ed}) - \theta(\boldsymbol{J}) \right\|_2^2 \tag{8}$$

式中，θ为边缘检测器用“两层卷积 + ReLU”结构近似模拟Sobel算子，分别提取$\boldsymbol{J}_{ed}$和$\boldsymbol{J}$的边缘信息图，可以有效促使模型学习图像中的边缘信息。

2　实　验

2.1　数据集与指标

为全面验证所提方法在遥感图像去雾中的有效性与鲁棒性，本文选取了三个具有代表性的公开数据集进行实验评估，分别为SateHaze1k（Huang等，2020）、HRSD（Zhang等，2022）和RRSHID（Zhu等，2025）。SateHaze1k数据集包含1200对配准良好的有雾/无雾遥感图像对，并按照雾浓度划分为薄雾（Thin）、中雾（Moderate）和浓雾（Thick）三个子集。HRSD数据集由多区域真实遥感雾图像构成，具有分辨率高、地物类型丰富以及雾分布复杂等特点。RRSHID是一个大规模的真实遥感图像去雾数据集，覆盖多种地理区域和大气条件，其雾分布高度非均匀，是目前公认的高难度评测基准之一。上述数据集涵盖了从合成雾到真实雾场景、从均匀雾分布到强非均匀雾分布等多种复杂情形，能够较为全面地反映模型在实际遥感应用中的性能表现。

在评价指标方面，本文同时采用有参考与无参考图像质量评价标准，从多个维度对去雾结果进行综合评估。具体而言，选用PSNR和SSIM衡量去雾图像与参考清晰图像在像素层面和结构层面的接近程度，同时，引入FADE对无参考场景下的残留雾感进行评估。三者结合能够较为全面地反映模型在图像清晰度、结构一致性以及主观视觉质量方面的综合性能。各指标的具体计算方式如下：PSNR基于MSE计算，其定义为

$$MSE = \frac{1}{H \times W} \sum_{i=1}^{H} \sum_{j=1}^{W} (\boldsymbol{I}(i,j) - \boldsymbol{I}_{gt}(i,j))^2,$$
$$PSNR = 10 \times \log_{10}\left(\frac{1.0^2}{MSE}\right) \tag{9}$$

式中，H和W分别为图像的高度和宽度，$\boldsymbol{I}(i,j)$为去雾图像在(i,j)处的像素值，$\boldsymbol{I}_{gt}(i,j)$为清晰参考图像的对应像素值。SSIM从亮度、对比度和结构三个维

度评估图像相似度，其定义为

$$SSIM(\boldsymbol{I},\boldsymbol{I}_{\mathrm{gt}})=\frac{(2\mu_I\mu_{I_{\mathrm{gt}}}+C_1)(2\sigma_{II_{\mathrm{gt}}}+C_2)}{(\mu_I^2+\mu_{I_{\mathrm{gt}}}^2+C_1)(\sigma_I^2+\sigma_{I_{\mathrm{gt}}}^2+C_2)} \tag{10}$$

式中，μ_I和$\mu_{I_{\mathrm{gt}}}$分别为$\boldsymbol{I}$和$\boldsymbol{I}_{\mathrm{gt}}$的均值，$\sigma_I^2$和$\sigma_{I_{\mathrm{gt}}}^2$分别为两者的方差，$\sigma_{II_{\mathrm{gt}}}$为两者的协方差，$C_1$和$C_2$为避免分母为0的常数，分别定义为

$$C_1=(0.01\times 1.0)^2, C_2=(0.03\times 1.0)^2$$

FADE是无参考指标，其定义为

$$L_{var}=Var(Laplacian(\boldsymbol{G})), C_{std}=Std(\boldsymbol{G})$$

$$FADE=\frac{1}{L_{var}\times 0.001+C_{std}\times 0.01+10^{-6}} \tag{11}$$

式中，$\boldsymbol{G}$为去雾图像对应的灰度图，L_{var}代表拉普拉斯算子提取的图像高频信息方差，C_{std}表灰度图的全局对比度标准差，该指标数值越小表明图像残留雾感越低。

2.2 实验设置

DMEGD-Net基于PyTorch框架并在NVIDIA GeForce RTX A5000 GPU平台上完成训练与测试。针对不同数据集的规模与特性，本文采用了差异化的训练策略：对于SateHaze1k和RRSHID数据集中的各子集，训练轮数设置为600；HRSD数据集的每个子集训练50轮。训练过程中，批量大小设置为4（SateHaze1k和HRSD）或8（RRSHID），初始学习率为1e-4，并采用Adam优化器对网络参数进行更新。同时，引入余弦退火学习率调度策略，以在训练后期逐步减小学习率，从而提升模型的收敛稳定性与最终性能。为增强模型的泛化能力，训练阶段对输入图像进行随机裁剪和水平翻转等数据增强操作。除非特别说明，所有对比方法均采用其原文中推荐的参数配置，并在相同的测试集上进行评估，以保证对比结果的公平性。

2.3 定量评估

本文在SateHaze1k、HRSD和RRSHID三个数据集上，将DMEGD-Net与多种代表性的传统方法及深度学习方法进行了对比实验，其中DCP是传统方法，AOD-Net、GridDehazed-Net、FFA-Net、FCTF-Net（Li等，2021）、自定进度半课程注意力网络（self-paced semi-curricular attention network，SCA-Net）（Guo等，2023）、PhD-Net、AU-Net、深度信息辅助的协作互促网络（depth information assisted collaborative mutual promotion network，DCMP-Net）（Zhang等，2024）和自适应一体化图像恢复（Adaptive all-in-one image restoration，AdaIR）（Cui等，2025）均为深度学习方法。所有方法均基于公开代码进行复现，并统一在对应数据集的测试集上计算指标。

如表1所示，DMEGD-Net在SateHaze1k数据集的不同雾浓度条件下均取得了最优或次优的表现。在Thin场景中，DMEGD-Net在PSNR和SSIM指标上均达到最优值（24.55dB/0.9111），表明其在薄雾条件下能够有效恢复图像细节。在Moderate场景中，DMEGD-Net因为兼顾图像整体性可能过多地平滑了局部的边缘，导致SSIM略低，但其PSNR相较于次优的PhD-Net（25.03dB）提升了0.46dB，说明模型在处理中雾时也具有一定优势。在最具挑战性的Thick场景中，DMEGD-Net依然保持了领先的指标，并显著高于AdaIR（21.67dB/0.8382），体现出较强的鲁棒性和稳定性。

如图4所示，DMEGD-Net在三种雾浓度条件下均保持较低的FADE值，说明其在有效去雾的同时，能够较好地抑制残留雾感。

在HRSD数据集上的定量结果如表2所示。DMEGD-Net在两个子集上均取得了最高的PSNR和SSIM，同时FADE指标也保持在最低水平。尤其在雾分布复杂、地物结构多样的HRSD-DHID，本文方法相较于现有深度学习模型表现出更加稳定的性能提升，比PSNR指标次优的DCMP-Net（25.60dB）高出1.77dB，验证了其在真实遥感场景中的适用性。

如表3所示，随着雾浓度的增加，各方法性能差异逐渐拉大。在Thin和Moderate场景中，DMEGD-Net在PSNR和SSIM上均处于领先水平；在Thick场景下，其优势更加明显，表明其在极端复杂大气条件下仍能够有效恢复图像结构与细节。

2.4 定性评估

除定量指标外，本文进一步通过主观视觉对比分析DMEGD-Net的去雾效果。在SateHaze1k、HRSD和RRSHID数据集的测试集中选取若干具有代表性的样例，与多种主流方法进行对比，结果如图5至图12所示。

SateHaze1k数据集上，不同方法在薄雾（图5）、中雾（图6）和浓雾（图7）条件下的表现差异较为明显。传统方法（如AOD-Net）和部分深度学习方法（如AU-Net）普遍存在残留雾痕、颜色偏移或局部细节模糊的问题。而DMEGD-Net在三种场景下均能够较好地恢复图像对比度与颜色一致性，同时有效

表1　不同方法在SateHaze1k数据集上的定量对比结果

Table 1　Quantitative comparison of different methods on the SateHaze1k dataset

方法	Haze1k-Thin		Haze1k-Moderate		Haze1k-Thick	
	PSNR ↑	SSIM ↑	PSNR ↑	SSIM ↑	PSNR ↑	SSIM ↑
DCP(He等,2009)	20.57	0.8725	20.81	0.9039	15.81	0.7423
AOD-Net(Li等,2017)	17.19	0.8403	15.60	0.7592	15.09	0.7281
GridDehaze-Net(Liu等,2021)	23.30	0.9074	23.80	0.9252	19.78	0.8067
FFA-Net(Qin等,2020)	22.06	0.8987	24.46	0.9232	21.10	0.8313
FCTF-Net(Li等,2021)	18.91	0.8496	21.62	0.8927	17.58	0.7675
SCA-Net(Guo等,2023)	23.37	0.8946	23.16	0.8294	20.33	0.8114
PhD-Net(Lihe等,2024)	23.68	0.9024	25.03	0.9301	21.32	0.8229
AU-Net(Du等,2024)	22.70	0.8992	21.05	0.9037	19.85	0.8226
DCMP-Net(Zhang等,2024)	23.35	0.8809	25.01	0.8929	20.56	0.7969
AdaIR(Cui等,2025)	24.43	0.9014	24.96	**0.9353**	21.67	0.8382
DMEGD-Net(本文)	**24.55**	**0.9111**	**25.49**	0.9295	**22.32**	**0.8441**

注:每列中最优结果以**加粗**显示,次优结果以下划线标记,"↑"表示值越大越好。

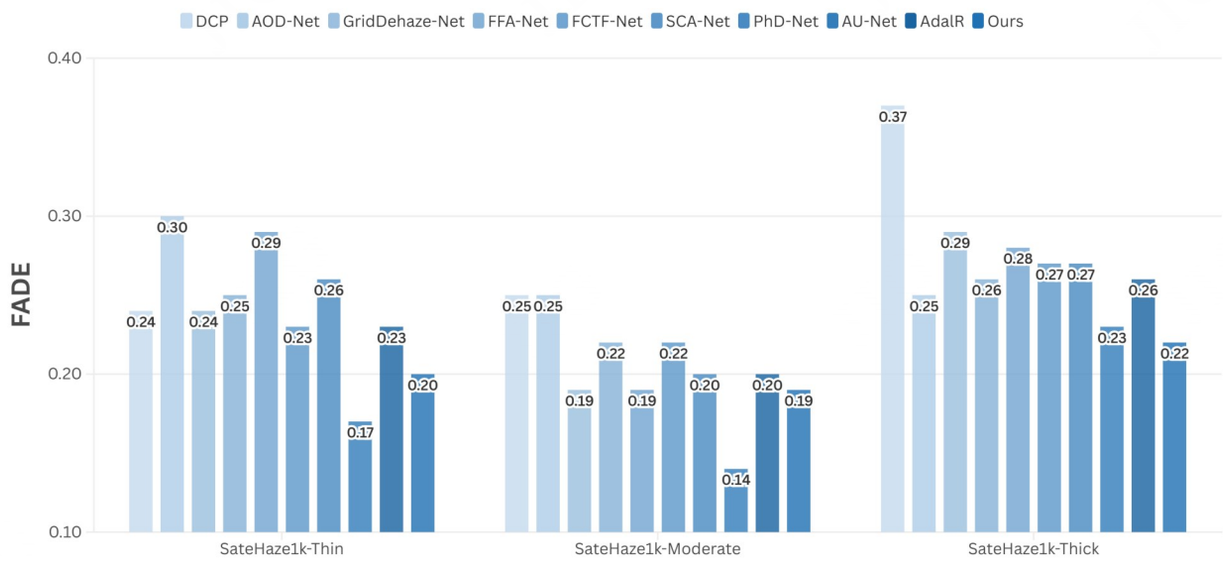

图4　不同方法在SateHaze1k数据集上FADE指标的柱状对比图

Fig. 4　Bar comparison of FADE metrics for different methods on the SateHaze1k dataset

保留植被、道路和建筑等区域的结构细节。

如图8和图9所示,在HRSD数据集上,由于雾分布更加复杂、地物结构多样且真实场景噪声较多,大多数方法(如FFA-Net、FCTF-Net和AdaIR等)在高雾密度区域仍存在明显残留。相比之下,DMEGD-Net借助CPA与DFB,在建筑边缘和道路轮廓等关键区域表现出更清晰的结构和更自然的色彩还原。

在RRSHID数据集上,去雾效果视觉对比如图10至12所示,各个方法面临的挑战进一步加大,如DCP、AOD-Net和AU-Net在所有浓度条件下的去雾图像均存在不同程度的伪影;AU-Net虽然在Moderate场景(图11)下略有改善,但出现了明显的色彩偏差,如第2行的屋顶颜色,Ground True为红色,而其去雾图像呈现为蓝色。而DMEGD-Net在不同雾浓度场景下均能够保持较稳定的视觉效果,尤其在

表2　不同方法在HRSD数据集上的定量对比结果

Table 1　Quantitative comparison of different methods on the HRSD dataset

方法	HRSD-DHID			HRSD-LHID		
	PSNR ↑	SSIM ↑	FADE ↓	PSNR ↑	SSIM ↑	FADE ↓
DCP(He等,2009)	18.90	0.8204	0.75	20.51	0.7870	**0.52**
AOD-Net(Li等,2017)	15.87	0.7233	0.86	21.73	0.8482	0.78
GridDehaze-Net(Liu等,2021)	24.64	0.8663	0.58	24.12	0.8816	0.62
FFA-Net(Qin等,2020)	22.73	0.8485	0.68	26.78	0.8949	0.63
FCTF-Net(Li等,2021)	22.53	0.8521	0.70	26.94	0.8973	0.65
SCA-Net(Guo等,2023)	23.47	0.8485	0.66	25.99	0.8874	0.67
PhD-Net(Lihe等,2024)	25.59	0.8744	0.69	27.23	0.8972	0.60
AU-Net(Du等,2024)	23.70	0.8548	0.62	16.91	0.5889	1.08
DCMP-Net(Zhang等,2024)	25.60	0.8271	0.60	27.21	0.8990	0.57
AdaIR(Cui等,2025)	23.97	0.8652	0.67	24.10	0.8874	0.58
DMEGD-Net(本文)	**26.77**	**0.8918**	**0.57**	**27.50**	**0.9058**	**0.52**

注:每列中最优结果以**加粗**显示,次优结果以下划线标记,"↑"表示值越大越好,"↓"表示值越小越好。

表3　不同方法在RRSHID数据集上的定量对比结果

Table 3　Quantitative comparison of different methods on the RRSHID dataset

方法	RRSHID-Thin		RRSHID-Moderate		RRSHID-Thick	
	PSNR ↑	SSIM ↑	PSNR ↑	SSIM ↑	PSNR ↑	SSIM ↑
DCP(He等,2009)	16.15	0.4762	13.32	0.4771	12.43	0.4493
AOD-Net(Li等,2017)	18.22	0.4851	15.27	0.3924	15.10	0.3847
GridDehaze-Net(Liu等,2021)	22.55	0.6104	22.55	0.6475	23.84	0.7126
FCTF-Net(Li等,2021)	21.20	0.5579	21.72	0.6313	22.43	0.6686
PhD-Net(Lihe等,2024)	22.04	0.5920	22.27	0.6423	23.11	0.6728
MixDehaze-Net(Lu等,2024)	22.02	0.5667	22.44	0.6234	23.64	0.6728
AU-Net(Du等,2024)	17.51	0.3493	17.16	0.5300	15.55	0.4755
DCMP-Net(Zhang等,2024)	22.82	0.5512	22.98	0.5722	23.89	0.5759
AdaIR(Cui等,2025)	22.50	0.6005	23.00	0.6632	23.67	0.7062
DMEGD-Net(本文)	**22.97**	**0.6171**	**23.09**	**0.6655**	**24.58**	**0.7252**

注:每列中最优结果以**加粗**显示,次优结果以下划线标记,"↑"表示值越大越好。

Thick(图12)场景中,其颜色恢复的准确性和结构完整性明显优于其他对比方法,充分体现了动态多专家建模在真实遥感去雾任务中的优势。

2.5　消融实验

为系统分析各模块设计及损失函数对整体性能的影响,本文在HRSD-DHID和Haze1k-Moderate上开展了消融实验,相关结果如表4和表5所示。

表4展示了在基础U-Net架构上逐步引入各关键模块后的性能变化情况,其中Base表示不包含可变形卷积与各模块的基础U-Net架构并采用"卷积+归一化+激活函数"的结构代替各个模块构建而成。可以看出,引入LD-Conv后,模型的特征建模能力得到初步提升;进一步加入MEG后,模型对不同场景特征的适应性明显增强;CPA的引入使模型更加关注关键区域,有效提升了结构一致性;最终结合DFB,模型在两个数据集上的PSNR和SSIM均取得

(a)有雾图像 (b)DCP (c)AOD-Net (d)GridDehaze-Net (e)FFA-Net (f)FCTF-Net (g)SCA-Net (h)PhD-Net (i)AU-Net (j)AdaIR (k)本文方法 (l)Ground Truth

图5　不同方法在SateHaze1k-Thin的去雾效果视觉对比

Fig. 5　Visual comparison of dehazing results by different methods on the SateHaze1k-Thin ((a)Haze Image; (b)DCP; (c)AOD-Net; (d)GridDehaze-Net; (e)FFA-Net; (f)FCTF-Net; (g)SCA-Net; (h)PhD-Net; (i)AU-Net; (j)AdaIR; (k)Ours; (l)Ground Truth)

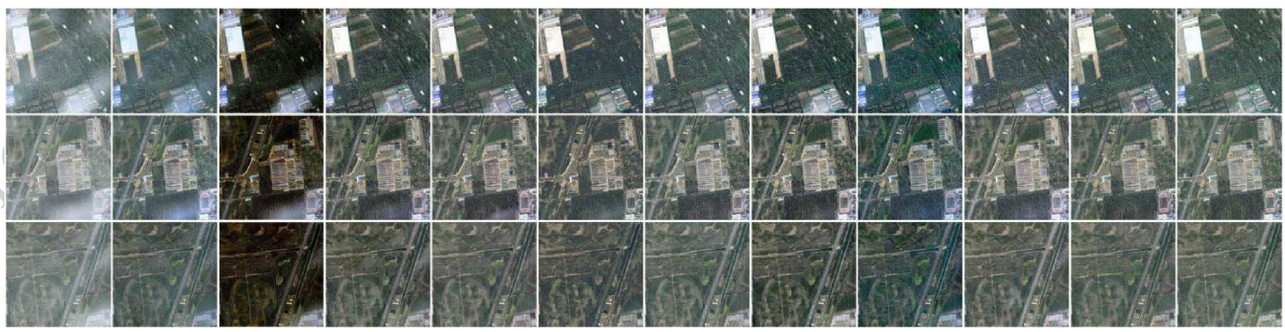

(a)有雾图像 (b)DCP (c)AOD-Net (d)GridDehaze-Net (e)FFA-Net (f)FCTF-Net (g)SCA-Net (h)PhD-Net (i)AU-Net (j)AdaIR (k)本文方法 (l)Ground Truth

图6　不同方法在SateHaze1k-Moderate的去雾效果视觉对比

Fig. 6　Visual comparison of dehazing results by different methods on the SateHaze1k-Moderate ((a) Haze Image; (b)DCP; (c)AOD-Net; (d)GridDehaze-Net; (e)FFA-Net; (f)FCTF-Net; (g)SCA-Net; (h)PhD-Net; (i)AU-Net; (j)AdaIR; (k)Ours; (l) Ground Truth)

(a)有雾图像 (b)DCP (c)AOD-Net (d)GridDehaze-Net (e)FFA-Net (f)FCTF-Net (g)SCA-Net (h)PhD-Net (i)AU-Net (j)AdaIR (k)本文方法 (l)Ground Truth

图7　不同方法在SateHaze1k-Thick的去雾效果视觉对比

Fig. 7　Visual comparison of dehazing results by different methods on the SateHaze1k-Thick ((a) Haze Image; (b)DCP; (c)AOD-Net; (d)GridDehaze-Net; (e)FFA-Net; (f)FCTF-Net; (g)SCA-Net; (h)PhD-Net; (i)AU-Net; (j)AdaIR; (k)Ours; (l) Ground Truth)

了最优性能,验证了各模块在整体性能提升中的协同作用。

在损失函数设计方面,表5对比了不同损失下模型的性能表现。实验结果表明,仅使用*L1*损失或

(a)有雾图像 (b)DCP (c)AOD-Net (d)GridDehaze-Net (e)FFA-Net (f)FCTF-Net (g)SCA-Net (h)PhD-Net (i)AU-Net (j)AdaIR (k)本文方法 (l)Ground Truth

图8　不同方法在HRSD-DHID的去雾效果视觉对比

Fig. 8　Visual comparison of dehazing results by different methods on the HRSD-DHID ((a) Haze Image; (b)DCP; (c)AOD-Net; (d)GridDehaze-Net; (e)FFA-Net; (f)FCTF-Net; (g)SCA-Net; (h)PhD-Net; (i)AU-Net; (j)AdaIR; (k)Ours; (l) Ground Truth)

(a)有雾图像 (b)DCP (c)AOD-Net (d)GridDehaze-Net (e)FFA-Net (f)FCTF-Net (g)SCA-Net (h)PhD-Net (i)AU-Net (j)AdaIR (k)本文方法 (l)Ground Truth

图9　不同方法在HRSD-LHID的去雾效果视觉对比

Fig. 9　Visual comparison of dehazing results by different methods on the HRSD-LHID ((a) Haze Image; (b)DCP; (c)AOD-Net; (d)GridDehaze-Net; (e)FFA-Net; (f)FCTF-Net; (g)SCA-Net; (h)PhD-Net; (i)AU-Net; (j)AdaIR; (k)Ours; (l) Ground Truth)

(a)有雾图像 (b)DCP (c)AOD-Net (d)GridDehaze-Net (e) FCTF-Net (f) PhD-Net (g)MixDehaze-Net (h)AU-Net (i)AdaIR (j)本文方法 (k)Ground Truth

图10　不同方法在RRSHID-Thin的去雾效果视觉对比

Fig. 10　Visual comparison of dehazing results by different methods on the RRSHID-Thin ((a) Haze Image; (b)DCP; (c)AOD-Net; (d)GridDehaze-Net; (e) FCTF-Net; (f)PhD-Net; (g)MixDehaze-Net; (h)AU-Net; (i)AdaIR; (j)Ours; (k) Ground Truth)

*L2*损失均难以同时兼顾整体视觉质量与局部结构恢复，而本文提出的*Lce*复合损失能够在两者之间取得更好的平衡，在两个数据集上均获得最高的PSNR和SSIM，进一步证明了该损失函数设计的在遥感图像去雾任务中的合理性与有效性。

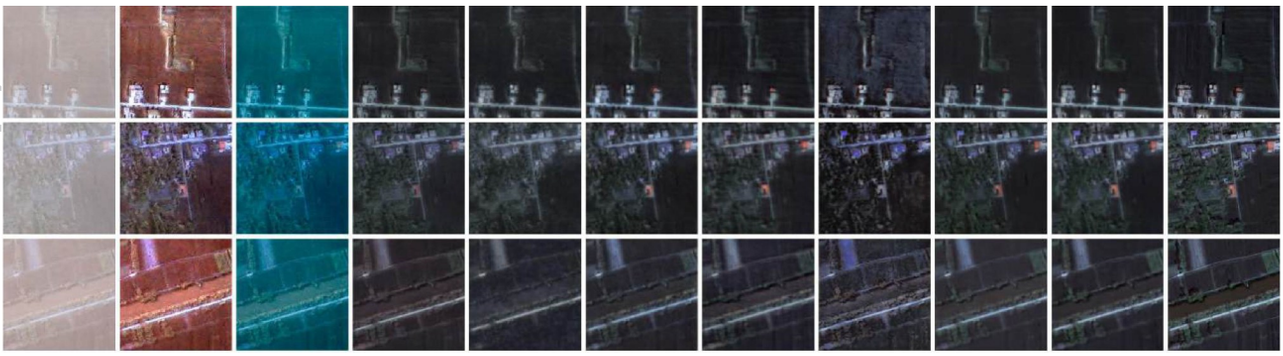

(a)有雾图像 (b)DCP (c)AOD-Net (d)GridDehaze-Net (e) FCTF-Net (f) PhD-Net (g)MixDehaze-Net (h)AU-Net (i)AdaIR (j)本文方法 (k)Ground Truth

图11　不同方法在RRSHID-Moderate的去雾效果视觉对比

Fig. 11　Visual comparison of dehazing results by different methods on the RRSHID-Moderate ((a) Haze Image; (b)DCP; (c)AOD-Net; (d)GridDehaze-Net; (e) FCTF-Net; (f)PhD-Net; (g)MixDehaze-Net; (h)AU-Net; (i)AdaIR; (j)Ours; (k) Ground Truth)

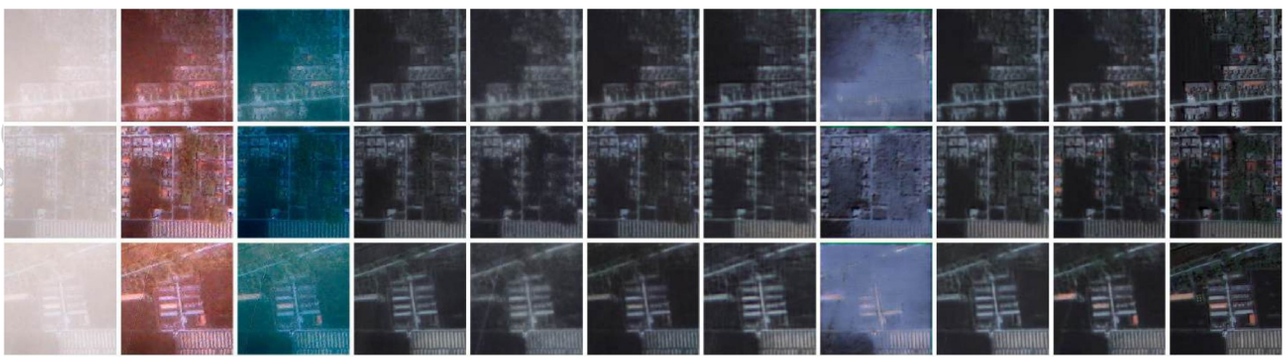

(a)有雾图像 (b)DCP (c)AOD-Net (d)GridDehaze-Net (e) FCTF-Net (f) PhD-Net (g)MixDehaze-Net (h)AU-Net (i)AdaIR (j)本文方法 (k)Ground Truth

图12　不同方法在RRSHID-Thick的去雾效果视觉对比

Fig. 12　Visual comparison of dehazing results by different methods on the RRSHID-Thick ((a) Haze Image; (b)DCP; (c)AOD-Net; (d)GridDehaze-Net; (e) FCTF-Net; (f)PhD-Net; (g)MixDehaze-Net; (h)AU-Net; (i)AdaIR; (j)Ours; (k) Ground Truth)

表4　模块组成对模型性能影响

Table 4　Effect of module composition on model performance

方法	HRSD-DHID		SateHaze1k-Moderate	
	PSNR ↑	SSIM ↑	PSNR ↑	SSIM ↑
Base	23.61	0.7968	23.09	0.8871
Base (LD)	24.48	0.8497	24.11	0.9092
Base (LD)+MEG	24.94	0.8552	24.48	0.9150
Base (LD)+MEG+CPA	25.60	0.8629	24.99	0.9290
Base (LD)+MEG+CPA+DFB	**26.77**	**0.8918**	**25.49**	**0.9295**

注:“↑”表示值越大越好。

表5　不同损失函数对模型性能的影响

Table 5　Effect of different loss functions on model performance

损失函数	HRSD-DHID		SateHaze1k-Moderate	
	PSNR ↑	SSIM ↑	PSNR ↑	SSIM ↑
*L1*损失	25.90	0.8766	24.47	0.9175
*L2*损失	26.34	0.8770	24.75	0.9216
*Lce*损失	**26.77**	**0.8918**	**25.49**	**0.9295**

注:“↑”表示值越大越好。

3　结　论

本文针对遥感图像在非均匀雾条件下易出现的颜色失真与结构退化问题,提出了一种基于动态多

专家门控机制的去雾网络(DMEGD-Net)。该网络通过动态门控网络实现颜色专家与边缘专家的自适应协同建模,使模型能够根据输入特征动态调节特征融合方式,从而提升对不同雾分布和复杂地物场景的表达能力。同时,引入通道-像素注意力模块和双源融合模块以增强关键区域感知能力,促进高层语义信息与低层结构细节的协同重建。结合内容损失与边缘约束构建的复合损失函数,引导模型在去雾过程中兼顾整体视觉质量与结构完整性。

在多个公开遥感图像数据集上的实验结果表明,所提方法在客观评价指标和主观视觉效果方面均优于现有主流方法,尤其在真实遥感场景和浓雾条件下表现出更稳定的去雾性能和更好的颜色与结构恢复能力。消融实验进一步验证了各模块设计的合理性与有效性。

尽管所提方法在去雾质量表现上取得了较好效果,但动态多专家结构在一定程度上增加了模型复杂度和计算开销。在处理高分辨率遥感图像时,模型对显存和推理时间的需求较高,在大规模遥感影像处理或实时应用场景中仍存在一定限制。未来工作将进一步探索模型轻量化设计,并加强物理成像约束与深度特征学习的融合,以提升模型在高分辨率遥感场景中的应用价值。

参考文献(References)

Berman D and Avidan S. 2016. Non-local image dehazing. Proceedings of the IEEE Conference on Computer Vision and Pattern Recognition (CVPR). Las Vegas, USA: IEEE: 1674 - 1682 [DOI: 10.1109/CVPR.2016.186]

Cai B L, Xu X, Jia K, Qing C M and Tao D C. 2016. DehazeNet: An end-to-end system for single image haze removal. IEEE Transactions on Image Processing, 25(11): 5187 - 5198 [DOI: 10.1109/TIP.2016.2598681]

Choi L K, You J and Bovik A C. 2015. Referenceless prediction of perceptual fog density and perceptual image defogging. IEEE Transactions on Image Processing, 24(11): 3888 - 3901 [DOI: 10.1109/TIP.2015.2456502]

Cui Y, Zamir S W, Khan S, Knoll A, Shah M and Khan F S. 2025. AdaIR: Adaptive all-in-one image restoration via frequency mining and modulation// Proceedings of the International Conference on Learning Representations (ICLR). Addis Ababa, Ethiopia: ICLR: (paper) [Best available DOI/index: arXiv:2403.14614]

Du Y, Li J, Sheng Q, Zhu Y X, Wang B and Ling X. 2024. Dehazing Network: Asymmetric Unet Based on Physical Model. IEEE Transactions on Geoscience and Remote Sensing, 62: 1 - 12 [DOI: 10.1109/TGRS.2024.3359217]

Fisher Y (ed.). 1995. Fractal image compression: Theory and application. Springer New York: New York, NY [DOI: 10.1007/978-1-4612-2472-3]

Fu X, Zeng D, Huang Y, Zhang X and Ding X. 2016. A weighted variational model for simultaneous reflectance and illumination estimation// Proceedings of the IEEE Conference on Computer Vision and Pattern Recognition. Las Vegas, USA: IEEE: 2782 - 2790 [DOI: 10.1109/CVPR.2016.304]

Gao L, Zhang B, Li W, Wang Y and Hu F. 2020. Dehazing of remote sensing images: A benchmark and beyond. ISPRS Journal of Photogrammetry and Remote Sensing, 165: 208 - 224 [DOI: 10.1016/j.isprsjprs.2020.04.012]

Guo Y, Gao Y, Liu R W, Lu Y, Qu J, He S and Ren W. 2023. SCANet: Self-paced semi-curricular attention network for non-homogeneous image dehazing// Proceedings of the IEEE/CVF Conference on Computer Vision and Pattern Recognition Workshops (CVPRW). Vancouver, Canada: IEEE: 1885 - 1894 [DOI: 10.1109/CVPRW59228.2023.00186]

He K M, Sun J and Tang X O. 2009. Single image haze removal using dark channel prior. IEEE Transactions on Pattern Analysis and Machine Intelligence, 33(12): 2341 - 2353 [DOI: 10.1109/TPAMI.2010.168]

He Y, Li C, Li X. 2023. Remote sensing image dehazing using heterogeneous atmospheric light prior[J]. IEEE Access, 11: 18805-18820 [DOI: 10.1109/ACCESS.2023.3245074]

Hu W, Yuan G D, Dong C and Zhang Y. 2010. A new single-image dehazing method based on dark channel prior. Journal of Computer Research and Development, 47(12): 2117 - 2124 (胡伟, 袁国栋, 董朝, 张勇. 2010. 基于暗通道优先的单幅图像去雾新方法. 计算机研究与发展, 47(12): 2117 - 2124)

Hu J, Shen L and Sun G. 2018. Squeeze-and-excitation networks// Proceedings of the IEEE/CVF Conference on Computer Vision and Pattern Recognition. Salt Lake City, USA: IEEE: 7132 - 7141 [DOI: 10.1109/CVPR.2018.00745]

Huang B, Li Z, Yang C, Sun F and Song Y. 2020. Single satellite optical imagery dehazing using SAR image prior based on conditional generative adversarial networks// Proceedings of the IEEE Winter Conference on Applications of Computer Vision (WACV). Snowmass Village, USA: IEEE: 1795 - 1802 [DOI: 10.1109/WACV45572.2020.9093471]

Jacobs R A, Jordan M I, Nowlan S J and Hinton G E. 1991. Adaptive mixtures of local experts. Neural Computation, 3(1): 79 - 87 [DOI: 10.1162/neco.1991.3.1.79]

Jobson D J, Rahman Z and Woodell G A. 1997. A multiscale retinex for bridging the gap between color images and the human observation of scenes. IEEE Transactions on Image Processing, 6(7): 965 -

976[DOI:10.1109/83.597272]

Koschmieder H. 1924. Theorie der horizontalen Sichtweite. Beiträge zur Physik der freien Atmosphäre, 12: 33 - 55

Li B, Peng X, Wang Z, Xu J and Feng D. 2017. AOD-Net: All-in-one dehazing network. Proceedings of the IEEE International Conference on Computer Vision (ICCV). Venice, Italy: IEEE: 4770 - 4778[DOI:10.1109/ICCV.2017.511]

Li Y and Chen X. 2021. A coarse-to-fine two-stage attentive network for haze removal of remote sensing images. IEEE Geoscience and Remote Sensing Letters, 18(10): 1751 - 1755[DOI:10.1109/LGRS.2020.3006533]

Lihe Z, He J, Yuan Q, Jin X, Xiao Y, Li J and Zhang L. 2024. PhD-net: A novel physic-aware dehazing network for remote sensing images. Information Fusion, 106: 102277[DOI:10.1016/j.inffus.2024.102277]

Lin M, Chen Q and Yan S C. 2014. Network in network. Proceedings of the International Conference on Learning Representations (ICLR). Banff, Canada

Liu X J, Ma Y F, Shi Z W and Chen J. 2021. GridDehaze-Net: Attention-based multi-scale network for image dehazing. Proceedings of the IEEE International Conference on Computer Vision (ICCV). Montreal, Canada: IEEE: 7314 - 7323[DOI:10.1109/ICCV48922.2021.00725]

Lu Y H, Wang H T, Zhang Y and Li X. 2024. MixDehazeNet: Mixed structure dehazing network for remote sensing images. Proceedings of the International Joint Conference on Neural Networks (IJCNN). Yokohama, Japan: IEEE: 1 - 8

Matthew D Z, Zeiler and Fergus R. 2013. Visualizing and understanding convolutional networks. Proceedings of the European Conference on Computer Vision (ECCV). Zurich, Switzerland: Springer: 818 - 833[DOI:10.1007/978-3-319-10590-1_53]

Qin X, Wang Z, Bai Y, Xie X and Jia H. 2020. FFA-Net: Feature fusion attention network for single image dehazing. Proceedings of the AAAI Conference on Artificial Intelligence, 34(7): 11908 - 11915[DOI:10.1609/aaai.v34i07.6865]

Riquelme C, Puigcerver J, Mustafa B, Neumann M, Lewkowycz A and Houlsby N. 2021. Scaling vision with sparse mixture of experts// Proceedings of the 35th Conference on Neural Information Processing Systems (NeurIPS). Virtual: NeurIPS

Shazeer N, Mirhoseini A, Maziarz K, Davis A, Le Q, Hinton G and Dean J. 2017. Outrageously large neural networks: The sparsely-gated mixture-of-experts layer. Proceedings of the International Conference on Learning Representations (ICLR). Toulon, France

Tang K, Yang J Y and Wang J. 2022. Survey of single image dehazing. IEEE Transactions on Image Processing, 31: 431 - 448[DOI:10.1109/TIP.2021.3129574]

Wang W J, Chen F, Liu G L, Cheng H and Wang M Q. 2025. Image dehazing network based on dual-domain feature fusion. Journal of Image and Graphics, 30(11): 3665 - 3679(王炜嘉, 陈飞, 刘莞玲, 程航, 王美清. 2025. 基于双域特征融合的图像去雾网络. 中国图象图形学报, 30(11): 3665 - 3679)

Wang Z, Bovik A C, Sheikh H R and Simoncelli E P. 2004. Image quality assessment: From error visibility to structural similarity. IEEE Transactions on Image Processing, 13(4): 600 - 612[DOI:10.1109/TIP.2003.819861]

Zhang L B and Wang S. 2022. Dense haze removal based on dynamic collaborative inference learning for remote sensing images. IEEE Transactions on Geoscience and Remote Sensing, 60: 1 - 16[DOI:10.1109/TGRS.2022.3207832]

Zhang Q D, Chi J, Chen Y Y and Zhang C M. 2024. A multi-branch defogging network based on fog concentration classification and dark and bright channel priors. Journal of Computer Research and Development, 61(3): 762 - 779(张琪东, 迟静, 陈玉妍, 张彩明. 2024. 基于雾浓度分类与暗-亮通道先验的多分支去雾网络. 计算机研究与发展, 61(3): 762 - 779)[DOI:10.7544/issn1000-1239.202220812]

Zhang X, Song Y, Song T, Yang D, Ye Y, Liu J and Wei X. 2024. LDConv: Linear deformable convolution for improving convolutional neural networks. Image and Vision Computing, 149: 105190[DOI:10.1016/j.imavis.2024.105190]

Zhang Y F, Zhou S and Li H F. 2024. Depth information assisted collaborative mutual promotion network for single image dehazing// Proceedings of the IEEE/CVF Conference on Computer Vision and Pattern Recognition (CVPR). Honolulu, HI, USA: IEEE: 2846 - 2855[DOI:10.1109/CVPR52733.2024.00275]

Zhu Q S, Mai J and Shao L. 2015. A fast single image haze removal algorithm using color attenuation prior. IEEE Transactions on Image Processing, 24(11): 3522 - 3533[DOI:10.1109/TIP.2015.2446191]

Zhu Z H, Lu W, Chen S B, Ding C H Q, Tang J and Luo B. 2025. Real-world remote sensing image dehazing: Benchmark and baseline. IEEE Transactions on Geoscience and Remote Sensing, PP(99): 1 - 1[DOI:10.1109/TGRS.2025.3584234]

Zuiderveld K. 1994. Contrast limited adaptive histogram equalization// Graphics Gems IV. San Diego, USA: Academic Press: 474 - 485

作者简介

施宇航,男,硕士研究生,主要研究方向数字图像处理。E-mail:yuhang@ahut.edu.cn

张骞,男,硕士研究生,主要研究方向为数字图像处理。E-mail:zhangqian@ahut.edu.cn

关鑫,男,博士研究生,主要研究方向为计算机视觉。E-mail:guanxin2020@email.swu.edu.cn